

This is the peer reviewed version of the following article:

Buckling of a Timoshenko beam bonded to an elastic half-plane: Effects of sharp and smooth beam edges / Falope, FEDERICO OYEDEJI; Lanzoni, Luca; Radi, Enrico. - In: INTERNATIONAL JOURNAL OF SOLIDS AND STRUCTURES. - ISSN 0020-7683. - 185-186:(2020), pp. 222-239. [10.1016/j.ijsolstr.2019.08.034]

Terms of use:

The terms and conditions for the reuse of this version of the manuscript are specified in the publishing policy. For all terms of use and more information see the publisher's website.

01/07/2024 07:35

(Article begins on next page)

Dear author,

Please note that changes made in the online proofing system will be added to the article before publication but are not reflected in this PDF.

We also ask that this file not be used for submitting corrections.



Contents lists available at ScienceDirect

International Journal of Solids and Structures

journal homepage: www.elsevier.com/locate/ijsolstr

Buckling of a Timoshenko beam bonded to an elastic half-plane: Effects of sharp and smooth beam edges

F.O. Falope^{a,c,*}, L. Lanzoni^{a,c,d}, E. Radi^{b,c}

^a University of Modena and Reggio Emilia, Dipartimento di Ingegneria "Enzo Ferrari", DIF, Via P. Vivarelli 10, Modena, 41125, Italy

^b University of Modena and Reggio Emilia, Dipartimento di Scienze e Metodi dell'Ingegneria, DISMI, Via G. Amendola 2, Reggio Emilia, 42122, Italy

^c CRICT - Centro Interdipartimentale di Ricerca e per i Servizi nel Settore delle Costruzioni, via P. Vivarelli 10, Modena, 41125, Italy

^d Centro Interdipartimentale "En&Tech", via G. Amendola, 2, Reggio Emilia, 42122, Italy

ARTICLE INFO

Article history:

Received 14 May 2019

Revised 25 July 2019

Accepted 27 August 2019

Available online xxx

Keywords:

Buckling load

Elastic half-plane

Edge effects

Timoshenko beam

Frictionless contact

Chebyshev polynomials

ABSTRACT

The problem of a compressed Timoshenko beam of finite length in frictionless and bilateral contact with an elastic half-plane is investigated here. A Chebyshev series solution is found and, for some limiting cases, an analytic form solution is provided. The problem formulation leads to an integro-differential equation which can be transformed into an algebraic system by expanding the rotation of the beam cross sections in series of Chebyshev polynomials. An eigenvalue problem is then obtained, whose solution provides the buckling loads of the beam and, in turn, the corresponding buckling mode shapes. Beams with sharp or smooth edges are considered in detail, founding relevant differences. In particular, it is shown that beams with smooth edges cannot exhibit a rigid-body buckling mode. A limit value of the soil compliance is found for beam with sharp edges, below which an analytic buckling load formula is provided without loss of reliability. Finally, in agreement with the Galin solution for the rigid flat punch on a half-plane, a simple relation between the half-plane elastic modulus and the Winkler soil constant is found. Thus, a straightforward formula predicting the buckling loads of stiff beams resting on compliant substrates is proposed.

© 2019 Published by Elsevier Ltd.

1 Introduction

The knowledge of the critical load of elastic bars, beams, plates, shell panels and layered systems bonded to a deformable support is a key task for many engineering problems with specific reference to foundation beams, bridge decks, end-bearing piles and thin-film based devices (MEMS and NEMS) or composite systems (Bazant and Cedolin, 2003; Foraboschi, 2009). The buckling problem is usually formulated as an eigenvalue problem, whose solution provides both the buckling loads and the corresponding mode shapes.

In general, the mechanical interaction between an elastic beam and the underlying substrate involves both shear and normal (peeling) stresses (Falope et al., 2018). However, in many practical applications the shear stress is usually small and thus it can be neglected according to the simplifying assumption of frictionless con-

tact (Reynolds, 1886). Moreover, the weight forces hinder the lifting of the beam from the substrate, thus making reasonable the assumption of bilateral contact for a wide class of practical cases.

The simplest model adopted in order to simulate an elastic support is the Winkler soil (WS). In this case, the support is represented by a series of discrete infinitesimal and mutually independent elastic springs. These springs provide to the beam axis a distributed transverse reactive pressure proportional to the beam deflection through the Winkler constant k . The soil stiffness is thus represented by a single substrate constant. As a consequence of its simplicity, many Authors extensively used such a scheme to investigate the buckling of beams on a deformable support (Timoshenko and Gere, 1961; Biot, 1957; Hetényi, 1971). Since its proposal, the Winkler model was subjected to a strong criticism by Wieghardt (1922) and many others owing to the fact that it leads to a rough approximation of the displacement field. Therefore, a non-local generalization of the Winkler model was later introduced by Wieghardt, who assumed that the contact pressure depends locally both on the deflection and curvature of the beam through two distinct parameters. The buckling problem of a beam laying on a Wieghardt soil was investigated in Smith (1969), Ruta and El-ishakoff (2006).

* Corresponding author at: University of Modena and Reggio Emilia, Dipartimento di Ingegneria "Enzo Ferrari", DIF, Via P. Vivarelli 10, 41125, Modena, Italy.

E-mail addresses: federicooyedeji.falope@unimore.it (F.O. Falope), luca.lanzoni@unimore.it (L. Lanzoni), enrico.radi@unimore.it (E. Radi).

Accurate analyses of the interaction between a beam and an underlying substrate can be performed by simulating the substrate (larger enough than the supported element) as a 2D semi-infinite elastic medium. Such an approach has been pursued by Shield and Kim (1992) in order to study an Euler-Bernoulli (E-B) beam resting on an incompressible elastic half-plane subjected to a uniform remotely applied strain. These authors also accounted for a shear-type cohesive zone at the interface in the neighbouring of the beam ends. Later, Lanzoni and Radi (2016) extended the analysis by considering a shear deformable Timoshenko beam resting on an elastic and isotropic half-plane and loaded by transversal forces. In this case, a complex power stress singularity is found at the beam ends, which depends on the Poisson ratio of the half-plane. Moreover, in proximity of the inner section of a Timoshenko beam loaded by a concentrated transversal force the pressure distribution between the beam and the half-plane displays a logarithmic singularity and the shear stress is finite and discontinuous across the loaded section, whereas for the E-B beam model the pressure was found regular therein. Accurate numerical studies about the interfacial stresses between bars and beams and an elastic 2D half-plane can be found in Tezzon et al. (2016), recently extended to a 3D half-space (Baraldi and Tullini, 2018).

The effect of a compressive load acting on an E-B beam resting on an elastic half-plane has been investigated by Gallagher (1974) by using a Chebyshev series expansion for representing the beam deflection. This Author considered special boundary conditions (BCs) for the beam, which was indeed assumed simply supported at the edges, hinged. However, the model of a continuum medium cannot sustain the concentrated loads that the supports can provide.

By using a coupled FE-BIE formulation involving the half-plane Green function, Tullini et al. (2012, 2013) numerically solved the buckling problem of Timoshenko beam in contact with an elastic half-plane under various BCs. Except for the Gallagher work (Gallagher, 1974), concerning E-B beam model, the aforementioned investigations are based on numerical approaches and, to Authors knowledge, a comprehensive analytical study on the stability of a Timoshenko beam bonded to an elastic half-plane cannot be found in Literature.

In the present work, the 2D problem of a compressed Timoshenko beam of finite length in frictionless and bilateral contact with an elastic and isotropic half-plane is investigated. Based on the relation between the interfacial reactive pressure and the displacement field, according to the Green function for an elastic half-plane loaded at its free surface, the problem is found to be governed by an integro-differential equation. The governing equation is then reduced to an algebraic system by expanding the rotation of the beam cross sections in series of Chebyshev polynomials of the first kind. Two dimensionless parameters, denoting the bending and shear stiffness of the beam with respect to (w.r.t.) that of the half-plane, completely characterize the system. The beam is considered free at its edges, thus requiring the vanishing of both the bending moment and the beam shear force resultant therein. Two different kinds of beam edges are considered in detail, namely sharp and smooth edges, which affect the distribution of the peeling stress within the contact region. For convenience, the corresponding eigenvalue problem for even and odd modes is formulated separately and then solved for the buckling loads. The results, provided in terms of fast convergent series expansion, show that the edge shape has a strong influence on the buckling load. In particular, it is shown that a beam with smooth edges can not exhibit a rigid-body critical buckling mode, differently from a beam with sharp edges.

The paper is organized as follows: The problem formulation and the BCs are presented in Section 2. The solution is worked out in Section 3 for even and odd buckling modes separately, whereas the

main results are reported and commented within Section 4. In particular, some reference cases have been analysed in Section 4.1. The convergence rate of the series solution varying the governing parameters has been also investigated therein. The buckling of a rigid beam resting on an elastic half-plane is discussed in Sections 4.2 and 4.3 and relevant differences are found between the two kinds of beam edges. Finally, conclusions are drawn in Section 5.

2. Problem formulation

2.1. Governing equations

Let us consider a Timoshenko beam of length $2a$ in frictionless and bilateral contact with an elastic half-plane. Two opposite compressive axial forces P act at the beam edges as sketched in Fig. 1.

The interfacial shear stress will be neglect in the following.¹

The plane problem is formulated per unit depth. The beam is characterized by the Young and shear moduli E_b and G_b , the moment of inertia I_b and the shear area $A_b^* = A_b/\chi$, being A_b the beam cross section area and χ its shear factor. The contact domain between the beam and the half-plane coincides with the entire beam length $2a$. The elastic half-plane is characterized by the Young modulus \bar{E}_h , being $\bar{E}_h = E_h/(1 - \nu_h^2)$ or $\bar{E}_h = E_h$ for plane strain or generalized plane stress, respectively, and ν_h is the Poisson ratio.

The reference system origin is placed at the middle-span of the beam with the x axis rightward directed along the contact region, as reported in Fig. 1. At the interface the beam is subjected to the peeling stress $q(x)$ exchanged with the underlying substrate. It is worth noticing that the effect of the compressive axial forces P is equivalent to a temperature load (Falope et al., 2016) ΔT according to $P = E_b h[(1 + \nu_h)\alpha_h - (1 + \nu_b)\alpha_b]\Delta T$ or $P = E_b h[\alpha_h - \alpha_b]\Delta T$ for plane strain or plane stress, respectively, where α_i represents the coefficient of thermal expansion and subscripts "h" and "b" denote the half-plane and beam amount.

For the Timoshenko beam, the beam deflection $v(x)$ and its cross sections rotation $\varphi(x)$ are related by the following kinematic relation

$$\varphi(x) = -v'(x) + \gamma(x), \quad (1)$$

where $\gamma(x)$ is the shear strain and the apex denotes differentiation w.r.t. the spatial variable x . The constitutive relations connecting the bending moment $M(x)$ and shear stress resultant $T(x)$ with the curvature $\varphi'(x)$ and shear compliance $\gamma(x)$ read

$$M(x) = E_b I_b \varphi'(x), \quad T(x) = G_b A_b^* \gamma(x). \quad (2)$$

For convenience, the vertical stress resultant $V(x)$ will be introduced in the following. Under the assumption of small deformations, the balance conditions of an infinitesimal beam element of length dx (see Fig. 2) in the deformed configuration yield the following relations (Timoshenko and Gere, 1961):

$$V'(x) = -q(x), \quad T(x) = M'(x) = V(x) + Pv'(x). \quad (3)$$

By combining Eqs. (1)–(3), a third-order ODE in the rotation field is found:

$$E_b I_b \left(1 - \frac{P}{G_b A_b^*}\right) \varphi'''(x) + P\varphi'(x) + q(x) = 0. \quad (4)$$

¹ The shear stress arising at the interface can be accounted for by introducing an additional compatibility condition between the beam and the half-plane strains along the x direction (Lanzoni and Radi, 2016). This leads to a strongly non-linear integro-differential equation which can be solved only by numerical approaches. Since the condition of shear has been neglected, the contact pressure is directly applied to the beam axis.

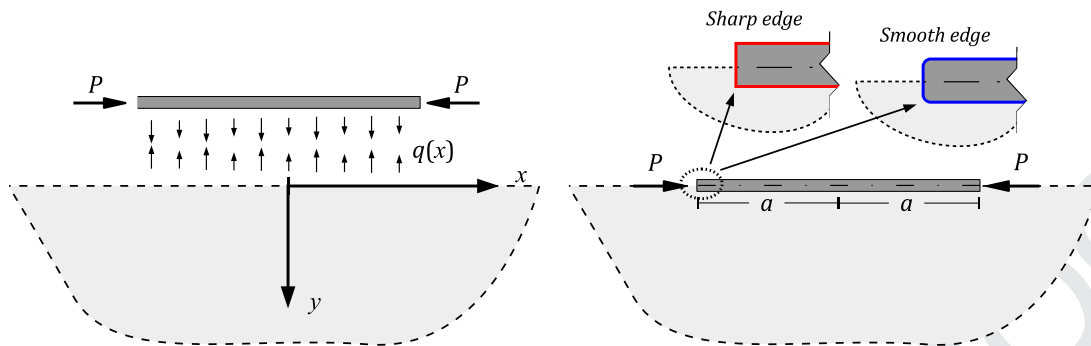


Fig. 1. Reference system.

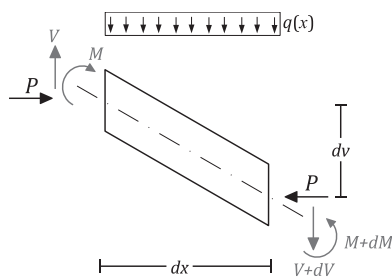


Fig. 2. Free-body diagram of an infinitesimal beam element in the deformed configuration.

150 The governing Eq. (4) highlights the coupling between the beam
151 and half-plane through the interfacial normal stress $q(x)$ (peeling
152 or pressure).

153 Two different kinds of beam edges are considered: *sharp edges*
154 and *smooth edges*, which induce (square-root) singular or vanishing
155 pressure at the edges, respectively, namely $q(\pm a) \rightarrow \infty$ or $q(\pm a) =$
156 0 . As known from Muskhelishvili (2013), the peeling stress can be
157 expressed as a function of the half-plane surface displacement ac-
158 cording to the Cauchy integral

$$q(x) = \frac{\bar{E}_h}{2\pi} \frac{1}{\mathcal{K}(x/a)} \int_{-a}^{+a} \frac{\mathcal{K}(t/a)}{t-x} v'(t) dt, \quad (5)$$

159 where

$$\mathcal{K}(t) = \begin{cases} \sqrt{1-t^2}, & \text{for sharp beam edges,} \\ 1, & \text{for smooth beam edges,} \\ \sqrt{1-t^2}, & \end{cases}$$

160 is here termed *edges function*.² By introducing the dimensionless
161 spatial variable $\xi = x/a$, based on Eqs. (1) and (5), the governing
162 Eq. (4) provides the following integro-differential equation for the
163 rotation field $\varphi(\xi)$

$$(1 - \tilde{P}\rho)\varphi'''(\xi) + \tilde{P}\varphi'(\xi) + \frac{\kappa}{2\pi} \frac{1}{\mathcal{K}(\xi)} \times \int_{-1}^{+1} \frac{\mathcal{K}(s)}{s-\xi} [\rho\varphi''(s) - \varphi(s)] ds = 0, \quad (6)$$

164 where $\tilde{P} = Pa^2/E_b I_b$ is the normalized axial load and

$$\kappa = \frac{\bar{E}_h a^3}{E_b I_b}, \quad \rho = \frac{E_b I_b}{a^2 G_b A_b^*}, \quad (7)$$

² Expression (5) for the peel stress follows from the solution of the problem of a rigid punch in frictionless contact with a half-plane (for details, see Muskhelishvili, 2013 p. 492–501) based on the use of complex potentials. As reported in Muskhelishvili (2013), function $\mathcal{K}(t/a)$ assumes different form depending on the presence of sharp or smooth edges of the punch profile. In particular, sharp edges are characterized by a singular pressure distribution, whereas smooth edges imply null pressure at the edge according to Hertz contact theory.

are two dimensionless parameters denoting the beam flexural 165
compliance compared to the half-plane stiffness and the ratio be- 166
tween the beam bending stiffness and shear stiffness, respectively. 167
In the following, κ and ρ will be called *stiffness parameter* and 168
shear parameter, respectively. 169

The beam edges are assumed as free. Accordingly, the BCs 170
require the bending moment M and vertical force V vanishing, 171
namely, by using Eqs. (2) and (3) 172

$$\varphi' = 0, \quad (1 - \tilde{P}\rho)\varphi'' + \tilde{P}\varphi = 0, \quad \text{for } \xi = \pm 1. \quad (8)$$

3. Problem solution 173

3.1. Solution strategy 174

The problem is approached by expanding the rotation field sec- 175
ond derivative $\varphi''(\xi)$ in series of Chebyshev polynomials of the first 176
kind $T_n(\xi)$. Once the integral pressure term (5) has been evaluated 177
in closed form, the governing equation is transformed into an in- 178
finite series of Chebyshev polynomials with unknown coefficients 179
 C_n . Then, the Galerkin procedure is applied by multiplying the gov- 180
erning equation by a set of appropriate functions and integrating 181
along the contact domain. In this way, by truncating the series at 182
the N th term, an algebraic system for the series expansion coef- 183
ficients is obtained and solved by using a suitable normalization 184
condition. This allows to achieve the buckling modes up to an ar- 185
bitrary amplitude constant. For convenience, in the following the 186
procedure is illustrated for even and odd modes, separately. 187

3.2. Even modes 188

In order to investigate the even modes, the second order deriva- 189
tive of the rotation field is expanded in series of Chebyshev poly- 190
nomials of the first kind, $T_n(\xi)$ with $n \in \mathbb{N}$ 191

$$\varphi''(\xi) = \sum_{n=1}^{\infty} C_{2n-1} T_{2n-1}(\xi), \quad (9)$$

where C_{2n-1} are the unknown coefficients. Higher and lower order 192
derivatives of Eq. (9) can be easily obtained by using relations 193
(31)–(33) provided in the Appendix A.1. Hence, the rotation field 194
and its derivatives involved in the governing Eq. (6) can be written 195
in terms of Chebyshev polynomials of the first and second kinds 196

$$\varphi'''(\xi) = \sum_{n=1}^{\infty} (2n-1)C_{2n-1} U_{2n-2}(\xi), \quad (10)$$

$$\varphi'(\xi) = \chi_0 + \frac{C_1}{4} T_2(\xi) + \frac{1}{4} \sum_{n=2}^{\infty} C_{2n-1} \left[\frac{T_{2n}(\xi)}{n} - \frac{T_{2n-2}(\xi)}{n-1} \right], \quad (11)$$

$$\begin{aligned} \varphi(\xi) = & \chi_0 T_1(\xi) + \frac{C_1}{24} [T_3(\xi) - 3T_1(\xi)] \\ & + \frac{C_3}{80} [10T_1(\xi) - 5T_3(\xi) + T_5(\xi)] \\ & + \frac{1}{8} \sum_{n=3}^{\infty} \frac{C_{2n-1}}{n[4(n-2)n^2 + n + 3]} \\ & \times [n(2n+1)T_{2n-3}(\xi) + (2n+1)(3-2n)T_{2n-1}(\xi) \\ & + (n-1)(2n-3)T_{2n+1}(\xi)], \end{aligned} \quad (12)$$

where χ_0 is an integration constant.

Due to the symmetry properties, it is sufficient to impose the BCs (8) at one edge only. Relations (8) are thus used to obtain the constant χ_0 and the coefficient C_3 in terms of the other unknown coefficients, namely

$$\begin{aligned} \chi_0 = & \frac{1}{4} \left[-C_1 + \frac{C_3}{2} + \sum_{n=3}^{\infty} \frac{C_{2n-1}}{(n-1)n} \right], \\ C_3 = & C_1 \frac{5\tilde{P}(3\rho+1) - 3}{3\tilde{P}(1-5\rho) + 5} + 5 \sum_{n=3}^{\infty} C_{2n-1} \frac{\tilde{P}[\frac{1}{3-4(n-1)n} + \rho] - 1}{\tilde{P}(1-5\rho) + 5}. \end{aligned}$$

The introduction of the series expansions (9) and (12) into the peeling stress distribution (5) provides

$$q(\xi) = \frac{\bar{E}_h}{2\pi} \frac{1}{\mathcal{K}(\xi)} \sum_{\substack{n=1 \\ n \neq 2}}^{\infty} C_{2n-1} \int_{-1}^{+1} \frac{\mathcal{K}(s)}{s-\xi} q_{2n-1}(s) ds, \quad (13)$$

where functions $q_{2n-1}(s)$ for $n = 1, 3, 4, \dots, \infty$ are listed in Appendix A.2. Depending on the edges function $\mathcal{K}(s)$, relations (34) and (35) for smooth or sharp edges are used to evaluate in closed form the integral in expression (13) (for details see Appendix A.2). As a consequence, the governing Eq. (6) is transformed into an infinite series of Chebyshev polynomials with unknown coefficients C_{2n-1} for $n = 1, 3, 4, \dots, \infty$

$$\sum_{\substack{n=1 \\ n \neq 2}}^{\infty} C_{2n-1} f_{2n-1}(\xi) = 0, \quad (14)$$

where functions $f_{2n-1}(\xi)$, defined in Appendix A.2, are linear combinations of Chebyshev polynomials and depend on the dimensionless axial load \tilde{P} as well as on the governing parameters ρ and κ .

In order to solve the governing Eq. (14) for the unknown coefficients, Eq. (14) is now multiplied by $T_m(\xi)/\sqrt{1-\xi^2}$ or $T_m(\xi)$, with $m = 1, 3, \dots$, for smooth or sharp edges, respectively, and then integrated for ξ ranging between -1 and 1 . Therefore, the following infinite eigensystem is derived in closed form

$$\mathbf{A}(\tilde{P})\mathbf{c} = \mathbf{0}, \quad (15)$$

where \mathbf{c} is Chebyshev coefficients vector and $\mathbf{A}(\tilde{P})$ is the system coefficient matrix defined in Appendix A.2. Then, the system characteristic Eq. (15), i.e. the buckling spectrum

$$\det[\mathbf{A}(\tilde{P})] = 0, \quad (16)$$

provides the eigenvalues \tilde{P}_i for $i = 1, 2, \dots, \infty$, i.e. the dimensionless buckling loads.

Once the eigenvalues are found from Eq. (16), the coefficients C_{2n-1} normalized w.r.t. the first coefficient C_1 are achieved. The displacement field follows by integrating relation (1) and the integration constant is found by imposing $v(\pm 1) = w(\pm 1, 0) = 0$, where $w(x, 0)$ is the vertical displacement of the half-plane surface loaded by the load distribution (13), namely (Muskhelishvili, 2013)

$$w(x, 0) = -\frac{2}{\pi \bar{E}_h} \int_{-a}^{+a} q(t) \ln|t-x| dt. \quad (17)$$

Table 1
Reference cases: dimensionless governing parameters.

Case	$\rho = \frac{E_h b}{G_b A_b a^2}$	$\kappa = \frac{\bar{E}_h a^2}{E_b b}$
1	0	15.625
2	0	1953
3	0.032	15.625
4	0.0036	1953
5	0	0.125

3.3. Odd modes

As for even modes, the odd modes are investigated by assuming the rotation field second order derivative series expansion of even Chebyshev polynomials as

$$\varphi''(\xi) = \sum_{n=0}^{\infty} C_{2n} T_{2n}(\xi). \quad (18)$$

Relations (31) and (32) in Appendix A.1 provide the derivatives of function $\varphi(\xi)$ up to the third order

$$\varphi'''(\xi) = \sum_{n=0}^{\infty} C_{2n} U_{2n-1}(\xi), \quad (19)$$

$$\varphi'(\xi) = \sum_{n=0}^{\infty} \frac{C_{2n}}{2} \left[\frac{T_{2n-1}(\xi)}{1-2n} + \frac{T_{2n+1}(\xi)}{2n+1} \right], \quad (20)$$

$$\begin{aligned} \varphi(\xi) = & \varphi_0 + \frac{1}{24} \left\{ 6C_0 T_2(\xi) - \frac{C_2}{2} [8T_2(\xi) + T_4(\xi)] \right. \\ & \left. + \sum_{n=2}^{\infty} C_{2n} \left[\frac{3T_{2n-2}(\xi)}{2n^2 - 3n + 1} + \frac{3T_{2n+2}(\xi)}{2n^2 + 3n + 1} - \frac{6T_{2n}(\xi)}{n(4n^2 - 1)} \right] \right\}. \end{aligned} \quad (21)$$

By imposing the BCs (8), the rigid rotation φ_0 and coefficient C_2 can be written as functions of the unknown coefficients C_{2n} for $n = 0, 2, 3, \dots, \infty$, namely

$$\begin{aligned} \varphi_0 = & 3 \left(C_0 + \sum_{n=2}^{\infty} \frac{C_{2n}}{1-4n^2} \right), \\ C_2 = & C_0 \frac{\tilde{P}(64\rho+3) - 64}{16\tilde{P}} \\ & - \sum_{n=2}^{\infty} C_{2n} \frac{64 + \tilde{P}[5 - 64(n^2 - 1)^2\rho] + n^2[64(n^2 - 2) + 7\tilde{P}]}{16(4n^4 - 5n^2 + 1)\tilde{P}}. \end{aligned}$$

Due to relations (18) and (21), the load term (5) becomes

$$q(\xi) = \frac{\bar{E}_h}{2\pi} \frac{1}{\mathcal{K}(\xi)} \sum_{\substack{n=0 \\ n \neq 1}}^{\infty} C_{2n} \int_{-1}^{+1} \frac{\mathcal{K}(s)}{s-\xi} q_{2n}(\xi) ds,$$

where functions $q_{2n}(\xi)$ for $n = 0, 2, 3, \dots, \infty$ are listed in Appendix A.2. Therefore, the governing Eq. (6) assumes the form of an infinite series of Chebyshev polynomials involving the unknown coefficients C_{2n} for $n = 0, 2, 3, \dots, \infty$, as

$$\sum_{\substack{n=0 \\ n \neq 1}}^{\infty} C_{2n} f_{2n}(\xi) = 0, \quad (22)$$

where functions $f_{2n}(\xi)$ for $n = 0, 2, 3, \dots, \infty$ are reported in Appendix A.2.

The solution is achieved by following the same procedure used for the even modes. The system coefficient matrix $\mathbf{A}(\tilde{P})$ and the Chebyshev coefficients vector \mathbf{c} are reported in Appendix A.2.

Table 2

Case 1 ($\rho = 0, \kappa = 15.625$): dimensionless buckling load p_i and edges effect parameter $\Pi_i = P_{i,Sh}/P_{i,Sm}$. Symbols $^{(o)}$ and $^{(e)}$ denote odd and even modes respectively.

Sharp edges				Smooth edges				Edges effect Π_i
Mode	Present Analysis		Tullini et al. (2013)	Mode	Series terms		Π_i	
	Series terms, N				4	10		
	4	5		4	10	12		
1 ^(e)	2.002	~	2.002	1 ^(e)	3.492	3.754	3.728	0.53
2 ^(o)	2.321	~	2.369	2 ^(o)	5.137	~	~	0.45
3 ^(o)	5.023	~	5.021	3 ^(e)	16.155	9.791	9.773	0.51
4 ^(e)	9.596	~	9.594	4 ^(o)	18.705	16.540	~	0.58

Table 3

Case 2 ($\rho = 0, \kappa = 1953.13$): dimensionless buckling load p_i and edges effect parameter $\Pi_i = P_{i,Sh}/P_{i,Sm}$. Symbols $^{(o)}$ and $^{(e)}$ denote odd and even modes respectively.

Sharp edges				Smooth edges				Edges effect Π_i
Mode	Present Analysis		Tullini et al. (2013)	Mode	Series terms		Π_i	
	Series terms, N				10	12		
	5	10		10	12	Π_i		
1 ^(e)	52.426	52.112	52.056	1 ^(e)	77.138	77.183	0.67	
2 ^(o)	52.172	~	52.117	2 ^(o)	78.324	~	0.66	
3 ^(o)	78.167	~	78.168	3 ^(o)	83.340	83.913	0.93	
4 ^(e)	80.606	79.513	79.511	4 ^(e)	85.839	85.911	0.93	

Table 4

Case 3 ($\rho = 0.032, \kappa = 15.625$): dimensionless buckling load p_i and edges effect parameter $\Pi_i = P_{i,Sh}/P_{i,Sm}$. Symbols $^{(o)}$ and $^{(e)}$ denote odd and even modes respectively.

Sharp edges				Smooth edges				Edges effect Π_i
Mode	Present Analysis		Tullini et al. (2012)	Mode	Series terms		Π_i	
	Series terms, N				4	10		
	4	5		4	10	12		
1 ^(e)	1.918	~	1.917	1 ^(e)	3.300	3.664	~	0.52
2 ^(o)	2.225	~	2.224	2 ^(o)	4.175	~	~	0.53
3 ^(o)	4.147	~	4.147	3 ^(e)	7.913	6.077	6.051	0.68
4 ^(e)	5.863	~	5.864	4 ^(o)	7.999	7.609	~	0.77

254 Then, the eigenvalues \tilde{P}_i for $i = 1, 2, \dots, \infty$ are determined as
 255 the roots of the characteristic Eq. (16) and the corresponding
 256 eigenvectors \mathbf{c}_i are obtained from the non-trivial solution of the
 257 homogeneous eigensystem (15) by introducing a suitable normal-
 258 ization w.r.t. the coefficient C_0 . Finally, the integration constant cor-
 259 responding to a rigid body motion is assessed by requiring $v(0) =$
 260 0, according to the skew-symmetry condition of the odd modes.

261 **4. Results and discussion**

262 The eigenvalues determined by solving the characteristic
 263 Eq. (16), for both odd and even modes as for sharp and smooth
 264 beam edges, are presented and discussed in the present section
 265 in terms of the governing dimensionless parameters. Attention is
 266 paid to the series expansions convergence. The edge effects on the
 267 buckling loads and mode shapes are investigated in detail.

268 Five reference cases have been considered, whose governing pa-
 269 rameters are reported in Table 1.

270 In order to validate the results provided by the present study,
 271 ρ and κ for cases 1 to 4 have been assumed corresponding to the
 272 cases numerically investigated in Tullini et al. (2012, 2013). In par-
 273 ticular, ρ and κ are related to the governing parameters αL and h/L
 274 used in Tullini et al. (2012, 2013) by the following relations:

$$\kappa = (\alpha L)^{\frac{3}{8}}, \quad \rho = \frac{4h}{5L}, \quad \text{with } L = 2a. \quad (23)$$

275 Cases 1 and 2 are representative of an E-B beam resting on a
 276 compliant and stiff half-plane respectively, whereas cases 3 and 4
 277 simulate a Timoshenko beam on a soft and stiff elastic half-plane
 278 respectively. The last case 5 corresponds to an E-B beam resting on
 279 a high compliant support. In this limit case, the beam is expected
 280 to buckle as a free beam, namely the first buckling load is almost
 281 vanishing and the corresponding buckling mode resembles a rigid
 282 body rotation. In the following, subscripts $_{Sh}$ and $_{Sm}$ denote a beam
 283 with sharp and smooth edges amount, respectively.

284 The results are reported in terms of the normalized buckling
 285 loads

$$p_i = \frac{P_i}{P_E} = \frac{4}{\pi^2} \tilde{P}_i,$$

286 namely the i th buckling load P_i is normalized w.r.t. the Euler criti-
 287 cal load $P_E = \pi^2 E_b J_b / 4a^2$ of a simply supported beam.

288 In the following, $\Pi_i = P_{i,Sh}/P_{i,Sm}$ will be defined the *edge effect*
 289 *parameter*, being the ratio between the eigenvalues obtained for
 290 a beam with sharp and smooth edges corresponding to the same
 291 mode number i .

292 **4.1. Buckling loads and modes**

293 The normalized eigenvalues p_i , for $i = 1 \div 4$, are reported in
 294 Tables 2–5 for cases 1 to 4. Symbol \sim denotes the convergence
 295 achievement. To be specific, we assume that convergence is at-

Table 5
Case 4 ($\rho = 0.0036$, $\kappa = 1953.13$): dimensionless buckling load p_i and edges effect parameter $\Pi_i = P_{i,Sh}/P_{i,Sm}$. Symbols ^(o) and ^(e) denote odd and even modes respectively.

Sharp edges			Smooth edges				
Mode	Present Analysis		Tullini et al. (2012)	Mode	Series terms		Edges effect Π_i
	Series terms, N						
	5	10		10	12		
1 ^(e)	46.770	46.362	46.342	1 ^(o)	70.181	~	0.66
2 ^(o)	46.416	~	46.399	2 ^(e)	70.267	70.439	0.66
3 ^(e)	72.839	70.400	70.400	3 ^(e)	72.068	73.705	0.95
4 ^(o)	70.776	~	70.776	4 ^(o)	73.134	~	0.96

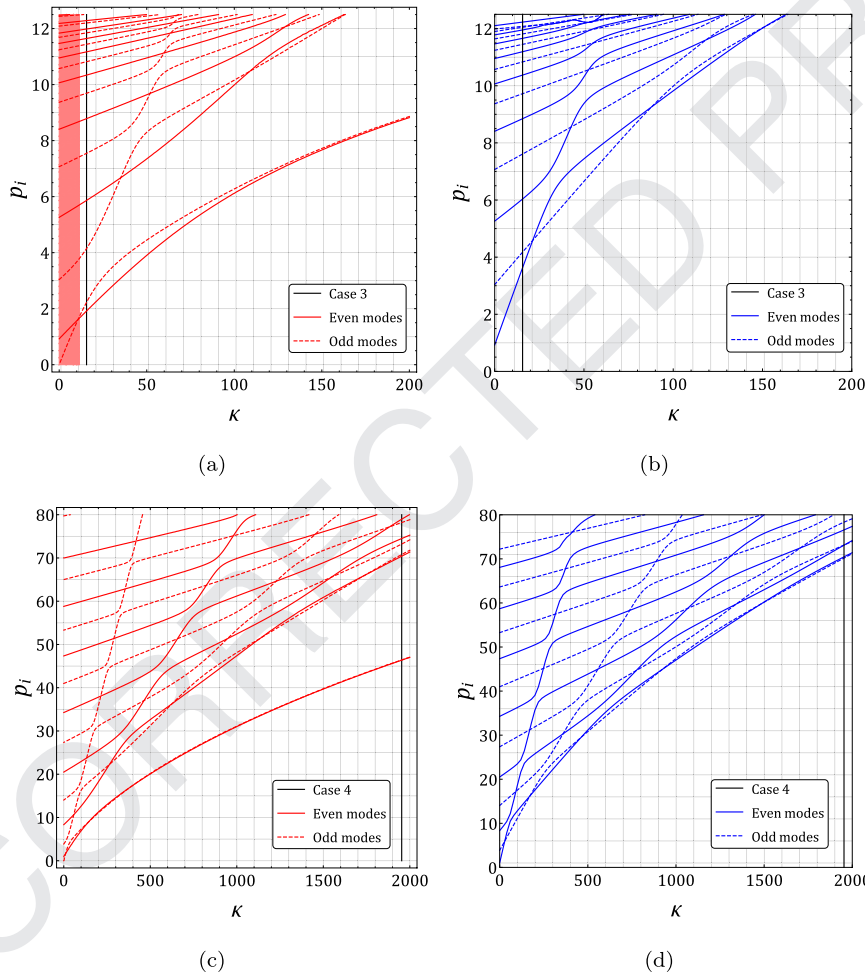


Fig. 3. The stiffness dimensionless parameter $\kappa = \bar{E}_h a^3 / E_p b$ influence on the dimensionless buckling loads: even modes (continuous lines) and odd modes (dashed lines). The red background highlights the $\kappa < \kappa_1$ region. (a) Beams with sharp edges: $\rho = 0.032$, low κ values; (b) Beams with smooth edges: $\rho = 0.032$, low κ values; (c) Beams with sharp edges: $\rho = 0.0036$, high κ values; (d) Beams with smooth edges: $\rho = 0.0036$, high κ values. (For interpretation of the references to colour in this figure legend, the reader is referred to the web version of this article.)

tained when the relative error between the solution obtained with N terms and that obtained with $N + 1$ terms is lower than 0.1%.
The convergence rate is influenced by the nature of the beam edges, the mode shape and the governing parameters. In particular, the convergence rate is faster for sharp edges than for smooth edges. Indeed, in case of smooth edges, a large number of terms is required for addressing the convergence, with the exception of the second odd mode, as shown in Tables 2–5. In addition, the convergence rate decreases as κ and ρ increase, specially for even modes.
Tables 2 and 4 show that the eigenvalues decrease as the shear parameter ρ increases as well as the stiffness parameter κ de-

creases. For small values of the parameter κ , the beam shear compliance has no relevant effects on the buckling load and mode. Indeed, in this case the buckling mode resembles a rigid body motion.
Conversely, the edges shape significantly affects the buckling loads, as shown in Tables 2–5 where the first four modes for cases 1–4 are reported. In particular, for low values of κ (stiff beams on compliant substrates), with special reference to the first mode shape, the parameter κ strongly influences the buckling load. The order in which the mode shape occurs, symmetric or skew, is also influenced by the edges shape. In particular, it can be observed from Tables 2–5 that only case 2 exhibits the same modes sort-

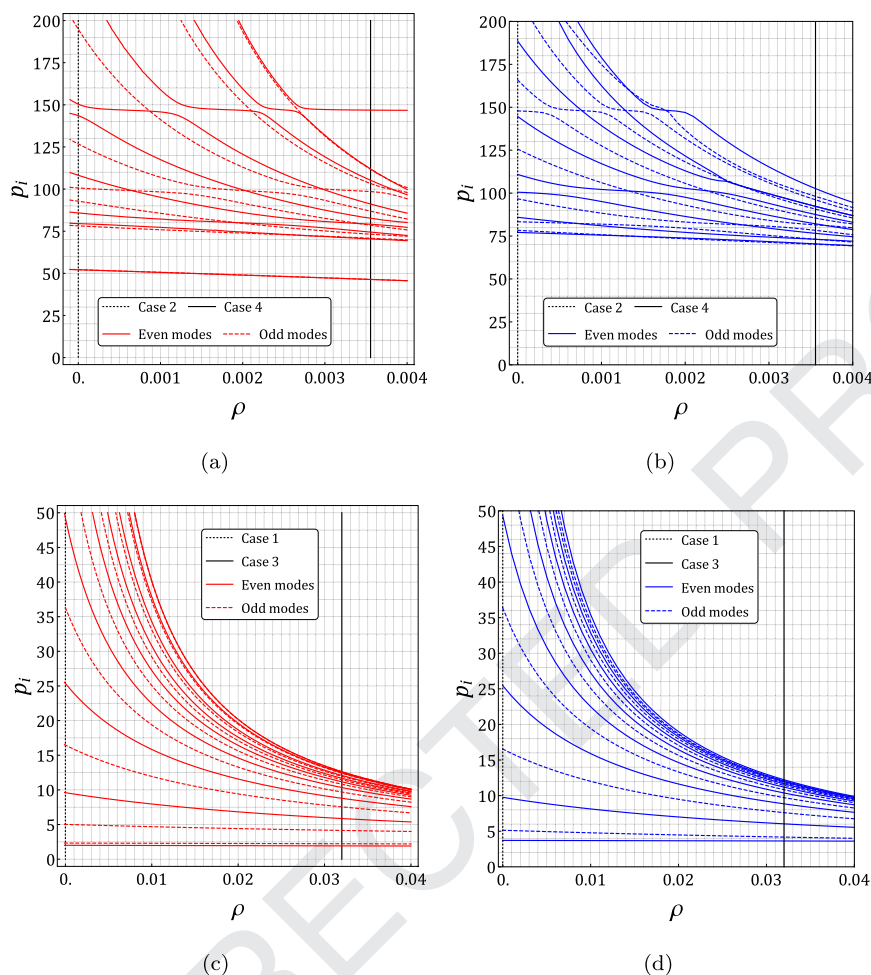


Fig. 4. The shear dimensionless parameter $\rho = E_b I_b / a^2 G_b A_b^*$ influence on the dimensionless buckling loads: even modes (continuous lines) and odd modes (dashed lines). (a) Beams with sharp edges: $\kappa = 1953$, low ρ values; (b) Beams with smooth edges: $\kappa = 1953$, low ρ values; (c) Beams with sharp edges: $\kappa = 15.625$, high ρ values; (d) Beams with smooth edges: $\kappa = 15.625$, high ρ values.

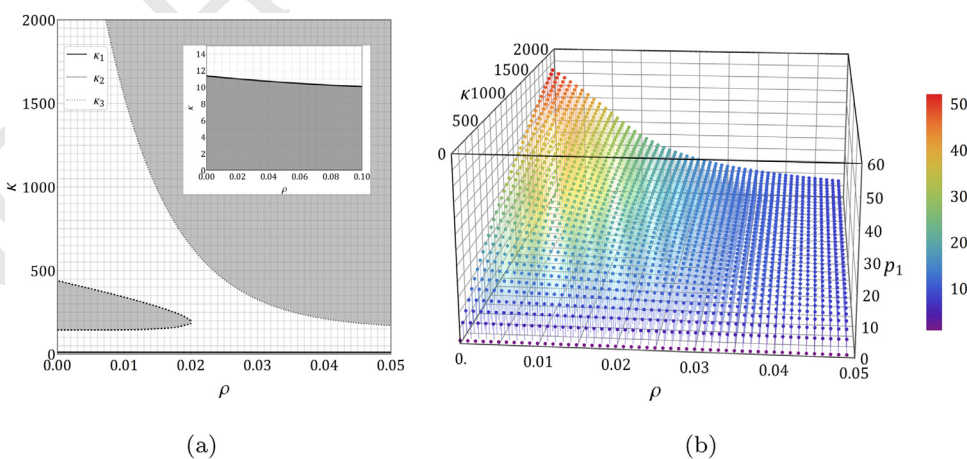


Fig. 5. First critical modes and corresponding buckling loads. (a) Nature of the first critical modes. Grey regions identify the occurrence of odd modes, white regions denote even modes; (b) Dimensionless first critical loads varying the governing parameters κ and ρ .

320 ing (alternated even and odd modes) both for sharp and smooth
 321 edges (symbols (o) or (e) denote odd or even modes, respectively).
 322 In all the other cases the mode sorting changes according to the
 323 kind of the beam edges.

324 The effects induced by the governing parameters are shown in
 325 Figs. 3 and 4, where the dimensionless buckling loads are plotted
 326 varying κ and ρ , for the considered reference cases.

327 Even and odd modes are plotted in solid and dashed lines, re-
 328 spectively, whereas red and blue lines represent sharp and smooth
 329 beam edges, respectively. Vertical black lines denote the reference
 330 cases of Table 1.

331 By comparing Fig. 3(a) and (c) for beams with sharp edges,
 332 with Fig. 3(c) and (d) concerning beams with smooth edges, a
 333 switch between even and odd modes is observed. In particular,

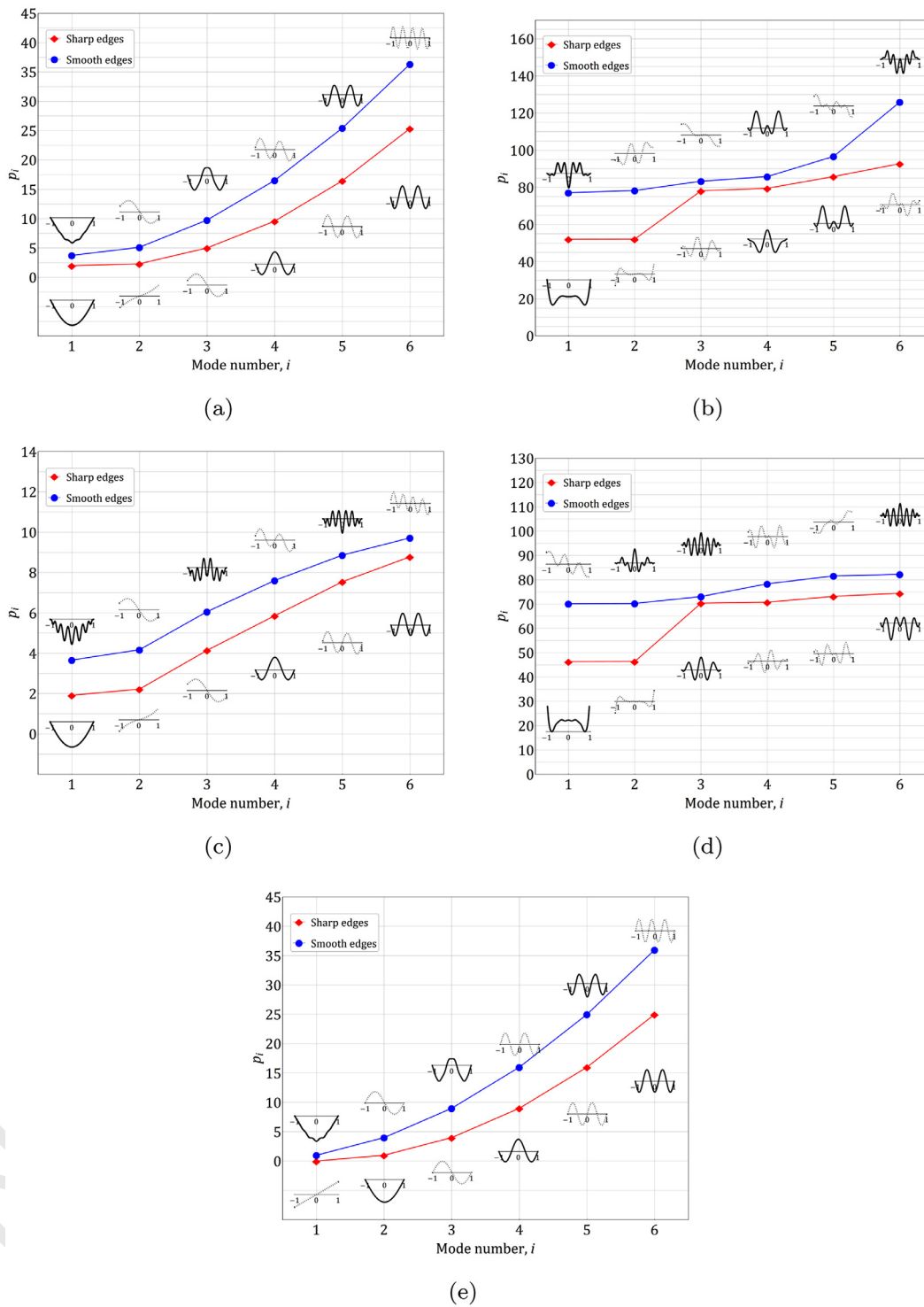


Fig. 6. Dimensionless buckling loads and associated buckling modes. (a) Case 1; (b) Case 2; (c) Case 3; (d) Case 4; (e) Case 5 (vanishing half-plane).

334 both for odd or even modes, the curves behave smoothly every-
 335 where except where they approached each other. Therein, instead
 336 of continuing smoothly and crossing, they suddenly deviate and do
 337 not intersect. Such a behaviour is known as *veering* phenomenon
 338 (Mace and Manconi, 2012). Conversely, the intersection points be-
 339 tween even and odd modes, denote the occurring of simultaneous
 340 even and odd modes under the same buckling load. The values of

κ corresponding to the intersection between the first odd and even 341
 342 modes will be denoted as κ_i . In particular, for a given value of the
 343 shear compliance ρ , the smallest value of κ_i will be denoted by
 344 κ_1 .

Making reference to case 3, for beams with sharp edges we 345
 346 found $\kappa_1 \cong 11.53$, as shown in Fig. 3(a). Therefore, for $\kappa < \kappa_1$ (com-
 347 pliant half-plane) the first buckling mode is odd and close to a

348 rigid rotation, whereas for $\kappa_1 < \kappa < \kappa_2$ the first buckling mode is
 349 even. Note also that for beams with smooth edges we obtained
 350 $\kappa_1 \cong 21.4$.

351 The buckling loads variation with the shear parameter ρ are
 352 reported in Fig. 4(a)–(d). For low values of ρ and high value of
 353 κ the veering phenomenon can be observed both for beams with
 354 sharp and smooth edges, as shown in Fig. 4(a) and (b), respectively.
 355 As the parameter ρ grows, the buckling loads and modes tend to
 356 approach each others, with special reference to higher modes, as
 357 shown in Fig. 4(c) and (d). Note also that the lowest even and odd
 358 modes are almost unaffected by the parameter ρ , as confirmed by
 359 the results listed in Tables 2–5.

360 The buckling modes and loads of beams with sharp edges are
 361 represented in Fig. 5(a) and (b), respectively, varying both the pa-
 362 rameters ρ and κ . In particular, for any couple of $\kappa - \rho$ values,
 363 grey or white regions of Fig. 5(a) characterize systems for which
 364 the first critical load is an odd or even mode, respectively. The de-
 365 tail in Fig. 5(a) shows that for $\rho < 0.1$, which is relevant for practi-
 366 cal cases, the first buckling mode is always odd for $\kappa < 10$. Further-
 367 more, the same detail emphasizes the negligible dependence of the
 368 first critical load p_1 on the shear parameter ρ for low values of κ .

369 The dimensionless plot of Fig. 5(b) provides the first buckling
 370 load p_1 as a function of the problem governing parameters. This
 371 plot highlights that the first critical loads are almost independent
 372 of the shear parameter ρ for low values of κ .

373 The first six buckling loads and modes corresponding to the
 374 considered reference cases are reported in detail in Fig. 6. In partic-
 375 ular, Fig. 6(c) and (d) show that the buckling modes of beams with
 376 smooth edges involve a larger wave number and higher buckling
 377 loads than beams with sharp edges.

378 Therefore, Fig. 6 together with the edge effect parameter $\Pi_i =$
 379 $P_{i,Sh}/P_{i,Sm}$, provided in Tables 2–5, always show that beams with
 380 smooth edges display higher buckling loads w.r.t. beams with
 381 sharp edges. Indeed, the edge effect parameter ranges between
 382 $0.5 \leq \Pi \leq 1$ and, referred to Fig. 6, the buckling loads curves of
 383 beams with smooth edges lay over the curves of beams with
 384 smooth edges for all the reference cases. Such a difference is more
 385 evident for cases 1 and 3 and for the first modes, for which a beam
 386 with smooth edges exhibits a critical load almost double of that of
 387 a beam with sharp edges.

388 A rigid-body like buckling mode does not occur for beams with
 389 smooth edges resting on a high compliant half-plane (see Fig. 6(e)).
 390 Conversely, Fig. 6(c) shows that beams with sharp edges resting on
 391 a high compliant half-plane exhibit a first odd buckling mode close
 392 to a rigid rotation. Such a trend is not observed for case 3, despite
 393 of the high compliance of the half-plane, $\rho = 0.032$. For such a situ-
 394 ation it is worth noticing that the buckling loads of beams with
 395 sharp and smooth edges tend to coincide as the mode number in-
 396 creases, accordingly to Fig. 4. Note also that when the half-plane
 397 stiffness is lower (cases 1, 5), the buckling loads approach those of
 398 an E-B simply supported beam, namely $p_i \approx n^2$.

399 4.2. Rigid beam resting on a compliant half-plane

400 The first buckling load of a rigid beam resting on a compliant
 401 substrate, namely as $\kappa \rightarrow 0^+$, is investigated in the present Sec-
 402 tion.

403 Looking for the solution of the governing Eq. (6) as a constant
 404 term ϕ_0 , the only non-vanishing term turns out to be the load con-
 405 tribute (5)³, namely

$$q(\xi) = \begin{cases} \frac{\bar{E}_h \phi_0}{2\pi} \frac{1}{\sqrt{1-\xi^2}} \int_{-1}^{+1} \frac{\sqrt{1-s^2}}{s-\xi} ds, & \text{for sharp edges,} \\ \frac{\bar{E}_h \phi_0}{2\pi} \sqrt{1-\xi^2} \int_{-1}^{+1} \frac{ds}{(s-\xi)\sqrt{1-s^2}}, & \text{for smooth edges.} \end{cases} \quad (24)$$

³ The identities $T_0(\xi) = U_0(\xi) = 1$ are used in (24).

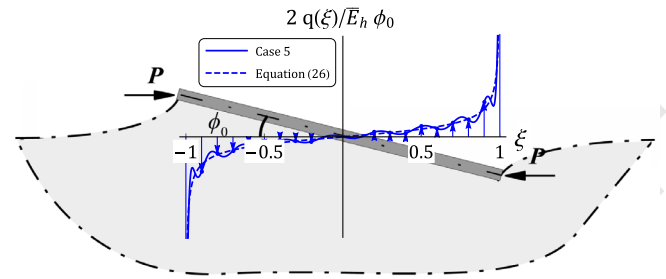


Fig. 7. Case 5: First mode pressure distribution. Series solution (solid line) vs closed form solution (dashed line).

406 However, by using Eq. (34) the pressure distribution (24) for beams
 407 with smooth edges is zero. Therefore, the moment generated by
 408 the axial loads P as a consequence of a rigid rotation ϕ_0 of the
 409 beam, namely

$$M_0 = 2\phi_0 Pa, \quad (25)$$

410 cannot be balanced by the soil reaction, except for $P = 0$, namely
 411 only the trivial solution is admitted. A rigid-like buckling mode
 412 cannot occur for beams with smooth edges.

413 Conversely, the peeling stress distribution (24) at the beam
 414 ends is singular for beams with sharp edges and, based on iden-
 415 tity (35), it reads

$$q_{Sh}(\xi) = -\frac{\bar{E}_h \phi_0}{2} \frac{\xi}{\sqrt{1-\xi^2}}. \quad (26)$$

416 Therefore, a square-root singular pressure, in agreement with
 417 Lanzoni and Radi (2016), takes place at the beam sharp edges and
 418 it can balance the external moment originated by the axial load P
 419 as a consequence of the rigid rotation ϕ_0 of the beam. A sketch of
 420 such a configuration is found in Fig. 7, where the dashed line de-
 421 notes the singular pressure distribution (26) whereas the solid line
 422 represents the pressure distribution obtained for the case 5. Both
 423 solutions have been normalized by $\phi_0 \bar{E}_h / 2$.

424 On the other hand, the overall moment generated by the pres-
 425 sure distribution (26) turns out to be

$$M_0 = 2a^2 \int_0^1 q(\xi) \xi d\xi = \frac{\pi \bar{E}_h \phi_0 a^2}{4}. \quad (27)$$

426 Moreover, by comparing Eqs. (25) and (27) the following relation
 427 between the overall moment and the rigid rotation is found

$$\phi_0 = \frac{4M_0}{\bar{E}_h \pi a^2},$$

428 in agreement with the well known Galin solution for a rigid flat
 429 punch resting on an elastic half-plane and subject to a couple M_0
 430 Kachanov et al. (2013).

431 A useful analytic design formula for the first buckling load,
 432 which holds for small values of κ , is provided by comparing
 433 (25) with (27), namely

$$p_{cr}^{(o)} \approx \frac{\bar{E}_h a \pi}{8} \text{ or } p_{cr}^{(o)} \approx \frac{\kappa}{2\pi}, \quad \text{for } \kappa < \kappa_1. \quad (28)$$

434 In particular, for case 5 ($\kappa = 0.125$ and $\rho = 0$), the design for-
 435 mula (28) provides a buckling load $p_{cr}^{(o)} = 0.198$, with a relative er-
 436 ror lower than 0.34% w.r.t. the provided series solution. Therefore,
 437 Eq. (28) can be used to predict the buckling loads of rigid beams
 438 resting on compliant substrates, i.e. for $\kappa < \kappa_1$.

439 4.3. Beam resting on a Winkler soil

440 The dimensionless buckling loads of an E-B beam resting on
 441 a Winkler soil (WS) are reported in Fig. 8(a) varying the WS di-

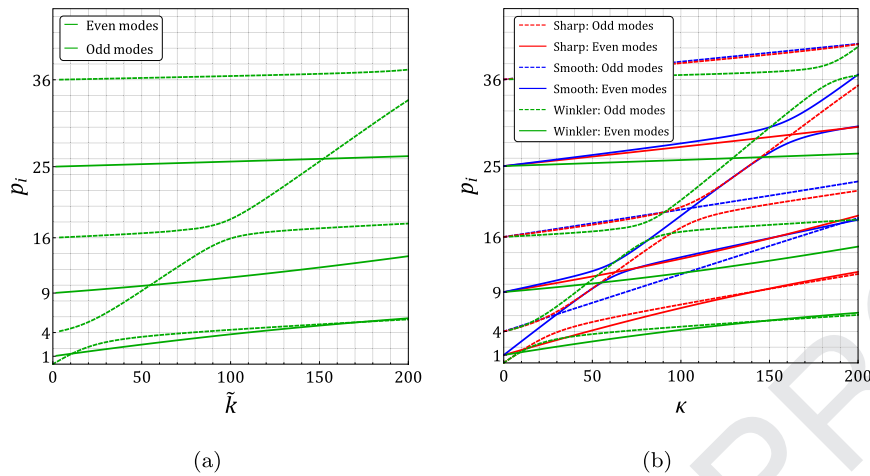


Fig. 8. (a) Dimensionless buckling loads of an E-B beam resting on a Winkler soil varying the parameter $\tilde{k} = ka^4/E_b I_b$; (b) Critical loads of an E-B beam supported by the Winkler soil compared with those of an E-B beam resting on an elastic half-plane by assuming $\tilde{k} = 3\pi\kappa/8$ according to Eq. (30).

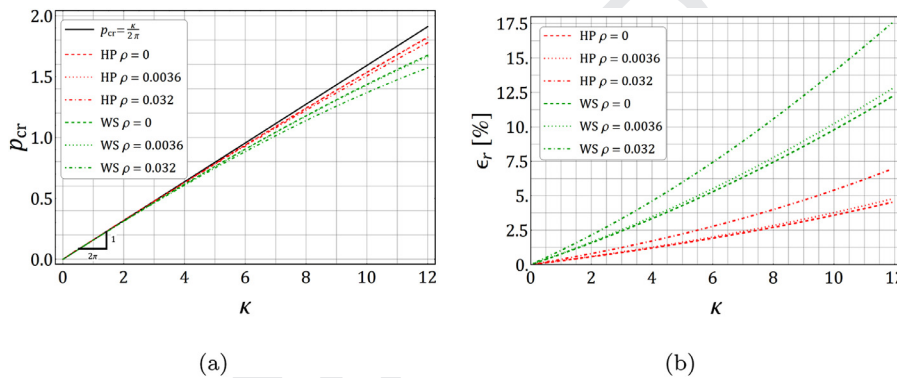


Fig. 9. (a) Dimensionless buckling loads p_{cr} predicted by Eq. (28) compared with the buckling loads of beams with sharp edges resting on a half-plane (HP) and on Winkler soil (WS) for different values of ρ ; (b) relative errors $\epsilon_r = 1 - P_i/P_i^{(0)}$ between Eq. (28) and the exact solution varying the parameter κ . (For interpretation of the references to color in the text, the reader is referred to the web version of this article.)

442 mensionless parameter $\tilde{k} = ka^4/E_b I_b$, being k the Winkler constant
 443 [Hetényi \(1971\)](#). As expected, as $\kappa \rightarrow 0^+$ the critical loads resemble
 444 those of a simply supported E-B beam ($p_i \approx n^2$). It is worth notic-
 445 ing that, similarly to the case of beams resting on a half-plane, the
 446 veering phenomenon occurs also for beams resting on a local soil.
 447 In particular, the trend of the first odd mode curve in [Fig. 8\(a\)](#) is
 448 close to that displayed in [Fig. 3\(a\)](#) concerning beams with sharp
 449 edges, both in terms of buckling loads and sorting of even-odd
 450 modes. This analogy is confirmed by [Fig. 8\(a\)](#), where the curves
 451 of [Fig. 8\(a\)](#) have been expressed w.r.t the half-plane problem gov-
 452 erning parameter κ and compared with the E-B beam bonded to
 453 an elastic half-plane dimensionless buckling load⁴ Note that, for all
 454 the observed values of κ , the slope of the curves representative of
 455 beams with smooth edges are always greater than those of beams
 456 with sharp edges, which in turn are greater than those of beams
 457 supported by a WS. Therefore, it seems that beams supported by a
 458 WS subjected to buckling exhibit a softer buckling behaviour w.r.t.
 459 beams resting on a half-plane. However it should be remarked that
 460 the governing parameter \tilde{k} differs from the stiffness parameter κ of
 461 a beam resting on an elastic half-plane. Indeed, in order to make a
 462 comparison between the results provided by the present approach
 463 for a beam on an elastic half-plane and those provided by the sim-
 464 plest WS assumption (as reported in [Fig. 8\(a\)](#)), it becomes neces-

sary to define a relation between the Winkler constant k and the
 half-plane elastic modulus \bar{E}_h . With this aim, the first buckling load
 obtained from the two substrate models are compared to obtain
 the required relation.

To be specific, for rigid beams resting on compliant substrates,
 in particular for $\kappa < \kappa_1$, a straightforward relation can be estab-
 lished between the Winkler constant k and the half-plane elastic
 modulus \bar{E}_h . Let us consider a flat punch on a WS subjected to a
 rotation ϕ_0 around its centre. Then, the interfacial pressure distri-
 bution assumes the form

$$q_{ws}(\xi) = -k\phi_0\xi a,$$

which implies an external moment M_0 given by

$$M_0 = \frac{2}{3}k\phi_0 a^3. \tag{29}$$

Thus, by comparing [Eqs. \(27\)](#) and [\(29\)](#), the following relation
 between the half-plane generalized Young modulus and the WS
 constant k holds

$$k = \frac{3\bar{E}_h}{8a}\pi, \quad \tilde{k} = \frac{3}{8}\pi\kappa. \tag{30}$$

Therefore, the buckling load of a rigid beam resting on a WS, which
 depends on the WS constant k [Hetényi \(1971\)](#), can be expressed
 as a function of the dimensionless stiffness parameter κ by using
 relation [\(30\)](#).

[Fig. 9 \(a\)](#) shows the buckling loads of a beam resting on a WS
[\(Hetényi, 1971\)](#) by using relation [\(30\)](#)₂ (green lines) and the buck-

⁴ In order to properly compared the WS buckling curves with those of a beam
 resting on a half-plane model, a relation between the half-plane elastic modulus
 and the Winkler constant, [Eq. \(30\)](#) will be provided in the present section.

485 ling load of beams with sharp edges resting on a half-plane (red
486 lines).⁵

487 As expected, formula (28) predicts reasonably well the first
488 bulking load for low values of κ , as shown in Fig. 9(a). The dis-
489 crepancy between formula (28) and the effective first buckling load
490 increases as κ and ρ increase, as reported in Fig. 9(b) where the
491 relative errors are shown reported. However, Fig. 9(b) shows that
492 for $\kappa < 12$, the relative error is lower than 20%, also for high values
493 of the shear parameter ρ . An alternative relation between the soil
494 constant k and the half-plane elastic modulus \bar{E}_h can be found in
495 Biot (1937).

496 5. Conclusion

497 The buckling analysis of a compressed Timoshenko beam with
498 sharp or smooth edges in bilateral and frictionless contact with an
499 elastic half-plane has been investigated. By expanding the rotation
500 field of the beam cross sections in series of Chebyshev polyno-
501 mials of the first kind, the governing integro-differential equation
502 has been transformed into an eigenvalue problem. This approach
503 has provided both the buckling loads and mode shapes as function
504 of the governing problem parameters, κ and ρ , the beam flexu-
505 ral compliance compared to the half-plane stiffness and the ratio
506 between the beam bending stiffness and its shear stiffness, respec-
507 tively. Five reference cases have been investigated in detail, and the
508 obtained results have been compared with those available in the
509 Literature, founding good agreement.

510 The influence of the stiffness parameter κ on the buckling load
511 is more relevant than the shear parameter ρ influence. Moreover,
512 the dependence of the buckling loads on the shear compliance is
513 more pronounced on the higher modes. It is worth noticing that
514 parameter κ affects also the sorting of the even or odd critical
515 modes.

516 It has been shown that beams with smooth edges can not
517 exhibit rigid-body like modes. Conversely, for beams with sharp
518 edges a particular value of the parameter κ , called κ_1 , has been in-
519 terpreted as a soil stiffness threshold for the occurrence of a rigid-
520 like mode. Indeed, for $\kappa < \kappa_1$ the first system buckling mode is odd
521 and closer to a rigid body rotation. On the other hand it has been
522 shown that for $\rho < 0.1$, the first mode exhibited by stiff beams on
523 compliant supports ($\kappa < 9$) is always odd.

524 A simple relation to predict the buckling loads of beams on
525 compliant substrate has been proposed also. In agreement with
526 the Galin solution for the rigid punch, a straightforward relation
527 between the Winkler soil constant and the half-plane elastic mod-
528 ulus holding for rigid beams has been found.

529 The dimensionless curves of Fig. 5 have been provided as a use-
530 ful design tool for the critical load evaluation.

531 The performed results can be used as a reliable support for
532 the design of layered systems characterized by high length-to-
533 thickness ratios, for which the instability phenomena represent the
534 main task. The challenging problem of a compressed beam in fric-
535 tional contact with an underlying elastic support will be handled
536 in a future work.

537 Acknowledgements

538 Financial support from the Italian Ministry of Education, Uni-
539 versity and Research (MIUR) in the framework of the Project
540 PRIN 2017 Modelling of constitutive laws for traditional and inno-
541 vative building materials (code 2017HFPKZY) is gratefully acknowl-
542 edged. Authors also acknowledge INdAM-GNFM "Gruppo Nazionale
543 di Fisica Matematica".

⁵ It is remarked that Eq. (30)₁ provides a relation between the half-plane modulus and the WS constant based on the rigid beam assumption. Therefore, relation (30)₁ does not involve the parameters κ and ρ .

544 **Appendix A**

545 *A1. Integral formulae involving Chebyshev polynomials*

546 The Chebyshev polynomials $T_n(x)$ and $U_n(x)$ of first and second kinds of order n are defined through the following identities

$$T_n(x) = \cos[n \arccos(x)],$$

$$U_n(x) = \frac{\sin[(n+1) \arccos(x)]}{\sin[\arccos(x)]},$$

547 with $0 \leq \arccos(x) \leq \pi$. The following relations of Chebyshev polynomials in the interval $[-1, 1]$ (Mason and Handscomb, 2002) have been
548 used:

$$T'_n(\xi) = n U_{n-1}(\xi), \tag{31}$$

$$\int T_n(x) dx = \begin{cases} \frac{1}{2} \left[\frac{T_{n+1}(x)}{n+1} - \frac{T_{n-1}(x)}{n-1} \right], & n \neq 1 \\ \frac{1}{4} T_2(x), & n = 1 \end{cases}, \tag{32}$$

$$T_n(\xi) = \frac{1}{2} [U_n(\xi) - U_{n-2}(\xi)] \tag{33}$$

$$\int_{-1}^1 \frac{T_n(x)}{\sqrt{1-x^2}(x-y)} dx = \text{sign}(n) \pi U_{n-1}(y), \tag{34}$$

$$\int_{-1}^1 \frac{\sqrt{1-x^2} U_n(x)}{x-y} dx = \begin{cases} \pi T_{n+1}(y), & \text{for } n \leq -2 \\ -\pi T_{n+1}(y), & \text{for } n > -2, \\ 0, & n = -1 \end{cases} \tag{35}$$

553 *A2. Problem known function and coefficient matrices*

554 The term involving the peeling stress $q(\xi)$ in the governing Eq. (6) can be decomposed as

$$q(\xi) = \frac{\kappa}{2\pi} \frac{1}{\mathcal{K}(\xi)} \int_{-1}^{+1} \frac{\mathcal{K}(s)}{s-\xi} \begin{cases} \sum_{\substack{n=1 \\ n \neq 2}}^{\infty} C_{2n-1} q_{2n-1}(s) ds, & \text{even modes} \\ \sum_{\substack{n=0 \\ n \neq 1}}^{\infty} C_{2n} q_{2n}(s) ds, & \text{odd modes} \end{cases} \tag{36}$$

555 where the introduced functions $q_i(s)$ turn out to be

$$q_1(s) = \frac{s}{3(\tilde{P} + 5\omega)} \left\{ 3[\omega(20\rho + 9) - 4] - \tilde{P} + s^2 \frac{\tilde{P} - 15\omega(2\rho + 1) + 10}{2} + s^4(3\omega - \tilde{P}) \right\},$$

$$q_{2n-1}(s) = s \left\{ \frac{\tilde{P}[6n(n-1)(10\rho + 1) + 3] + 5\omega(2n-3)(2n+1)[2(n-1)n(6\rho + 1) - 1]}{4n\{n[4n(n-2) + 1] + 3\}(\tilde{P} + 5\omega)} \right. \\ \left. + s^2 \frac{5(8\rho + 1)[\tilde{P} + \omega(2n-3)(2n+1)]}{2(3-2n)(2n+1)(\tilde{P} + 5\omega)} + \frac{s^4}{5} \left[\frac{4(n-2)(n+1)\tilde{P}}{(3-2n)(2n+1)(\tilde{P} + 5\omega)} + 1 \right] \right\} \\ + \frac{1}{8} \left\{ \frac{T_{2n-3}(s)}{n(5-2n)-3} - \frac{T_{2n+1}(s)}{n(2n^2+1)} + \left[\frac{1}{n(n-1)} + \rho \right] T_{2n-1}(s) \right\},$$

$$q_0(s) = \frac{4(3\omega - 1) - \tilde{P}}{2\tilde{P}} + (6\rho + 1)s^2 - \frac{s^4}{2},$$

$$q_{2n}(s) = 4n^2[\tilde{P} + \omega(4n^2 - 11) + 3] - \tilde{P} + 4(7\omega - 3) + s^2[6(1 - n^2)(4\rho + 1)\tilde{P} \\ + 2s^2\tilde{P}(n^2 - 1)] + \frac{T_{2n}(s)(n^2 - 1)[2\rho(4n^2 - 1) + 1]}{2[n^2(4n^2 - 5) + 1]} \\ + \frac{T_{2n+2}(s)(1-n)(2n-1) - T_{2n-2}(s)(n+1)(2n+1)}{8[n^2(4n^2 - 5) + 1]},$$

556 being $\omega = 1 - \tilde{P}\rho$. Therefore, based on relations (34) and (35), the governing integro-differential Eq. (6) is expressed in an infinite series
557 form

$$\sum_{\substack{n=1 \\ n \neq 2}}^{\infty} C_{2n-1} f_{2n-1}(\xi) = 0, \quad \text{for even modes} \\ \sum_{\substack{n=0 \\ n \neq 1}}^{\infty} C_{2n} f_{2n}(\xi) = 0, \quad \text{for odd modes} \tag{37}$$

558 where functions $f_1(\xi)$ and $f_{2n-1}(\xi)$ assume the following expressions for sharp or smooth beam edges

$$f_1(\xi) = \frac{1}{192(\tilde{P} + 5\omega)} \left\{ \frac{2\kappa[-5\tilde{P}(72\rho^2 + 1) + 8(45\rho - 7) + 159\omega]}{\sqrt{1 - \xi^2}} + 8\{(15\rho(24\rho + 13) + 8)\tilde{P}^2 - 3(7\omega + 65)\tilde{P} + 120[\omega(\omega + 6) - 3]\} \right\}, \text{ for sharp edges,}$$

$$f_1(\xi) = \frac{48[9\tilde{P} + 20(1 - 2\omega)] - 16[\rho(60\rho + 27) + 1]\tilde{P}^2 + \kappa\sqrt{1 - \xi^2}[3(80\rho^2 + 1)\tilde{P} - 15(16\rho - 7)\omega + 16]}{48(\tilde{P} + 5\omega)} - \xi^2 \left\{ \frac{\kappa\sqrt{1 - \xi^2}\{40(3\rho - 1) + 3[19\omega - 1\tilde{P}(40\rho^2 + 1)]\} - 60[(5 - \omega)\tilde{P} + 12(2\omega + 1)]}{12(\tilde{P} + 5\omega)} + \tilde{P}^2 \frac{5\rho(12\rho + 5) + 2}{\tilde{P} + 5\omega} \right\} + \xi^4 \frac{\kappa\sqrt{1 - \xi^2}(3\omega - \tilde{P}) + 10\tilde{P}(\tilde{P} - 3\omega)}{6(\tilde{P} + 5\omega)}, \text{ for smooth edges,}$$

559

$$f_{2n-1}(\xi) = \kappa \left\{ \frac{\tilde{P}[4n(n - 84\omega) + 3] + 4n\{10[4(n - 2)n^2 + n + 3]\rho\omega + n[8(n - 2)n - 13]\omega + 10(n - 1)\} + 15\omega}{16n[4(n - 2)n^2 + n + 3]\sqrt{1 - \xi^2}(\tilde{P} + 5\omega)} + \xi^4 \frac{[\tilde{P} + (2n - 3)(2n + 1)\omega][\kappa(20\rho + 3) - 10\sqrt{1 - \xi^2}\tilde{P}]}{2(2n - 3)(2n + 1)\sqrt{1 - \xi^2}(\tilde{P} + 5\omega)} + \xi^6 \frac{\kappa[\tilde{P} + (2n - 3)(2n + 1)\omega]}{2(3 - 2n)(2n + 1)\sqrt{1 - \xi^2}(\tilde{P} + 5\omega)} \right\} + \sqrt{1 - \xi^2} \left\{ \frac{-3\tilde{P}(\tilde{P} + 5\omega) - 2n[-3(30\rho^2 + 1)\tilde{P}^2 + 55\omega\tilde{P} - 180\omega + 90]}{4n[4(n - 2)n^2 + n + 3]\sqrt{1 - \xi^2}(\tilde{P} + 5\omega)} + n^2 \frac{2[-3(70\rho^2 + 1)\tilde{P}^2 + 35\omega\tilde{P} + 60\omega(4\omega - 7) + 210] + 80n\omega(\tilde{P} - 6\omega) + 40n^2\omega(6\omega - \tilde{P})}{4n[4(n - 2)n^2 + n + 3]\sqrt{1 - \xi^2}(\tilde{P} + 5\omega)} \right\} + U_{2n}(\xi) \frac{8(n - 1)(2n + 1)\sqrt{1 - \xi^2}\tilde{P} + \kappa + 8\kappa n(-2n^2 + n + 1)\rho - 4\kappa n}{64(n - 1)n(2n + 1)\sqrt{1 - \xi^2}} + \frac{\kappa U_{2(n+1)}(\xi)}{64n(2n + 1)\sqrt{1 - \xi^2}} + \frac{U_{2(n-1)}(\xi)}{64} \left[\kappa \frac{8n(2n - 3)\rho + 3}{n(2n - 3)\sqrt{1 - \xi^2}} - \frac{8\tilde{P}}{n - 1} \right] + \frac{U_{2(n-2)}(\xi)}{64(n - 1)(2n + 1)} \left[8\left(1 - 2n + \frac{1}{n}\right)\tilde{P} + \kappa \frac{8(n - 1)(2n + 1)\rho + 3}{\sqrt{1 - \xi^2}} \right] + \frac{\kappa U_{2(n-3)}(\xi)}{64[n(2n - 5) + 3]\sqrt{1 - \xi^2}}, \text{ for sharp edges,}$$

560

$$f_{2n-1}(\xi) = \frac{-5\{2(n - 1)n[4(n - 1)n - 11] + 3\}\omega\tilde{P} + [6(1 - n)n - 3]\tilde{P}^2 + 60n[4(n - 2)n^2 + n + 3]\omega^2}{4n[4(n - 2)n^2 + n + 3](\tilde{P} + 5\omega)} + \kappa\sqrt{1 - \xi^2} \frac{[5(n - 1)n + 6]\tilde{P} + (n - 1)n\{\omega[4(n - 1)n(40\rho + 13) - 120\rho - 119] + 40\} + 30\omega}{16n[4(n - 2)n^2 + n + 3](\tilde{P} + 5\omega)} + \xi^2 \frac{[\tilde{P} + (2n - 3)(2n + 1)\omega][120\omega - 15\tilde{P} + 2\kappa\sqrt{1 - \xi^2}(10\rho + 1)]}{2(3 - 2n)(2n + 1)(\tilde{P} + 5\omega)} + \xi^4 \frac{[\tilde{P} + (2n - 3)(2n + 1)\omega](\kappa\sqrt{1 - \xi^2} - 10\tilde{P})}{2(2n - 3)(2n + 1)(\tilde{P} + 5\omega)} + U_{2(n-1)}(\xi) \frac{\tilde{P}\{2 - 4n[8n(n - 1)\rho + 1]\} + \kappa\sqrt{1 - \xi^2} + 8n(n - 1)(\kappa\sqrt{1 - \xi^2}\rho + 4n - 2\omega)}{16n(n - 1)} + \frac{U_{2n}(\xi)}{32n} \left(4\tilde{P} - \frac{2\kappa\sqrt{1 - \xi^2}}{2n + 1} \right) + U_{2(n-2)}(\xi) \frac{2(2n - 3)\tilde{P} - \kappa\sqrt{1 - \xi^2}}{16[n(2n - 5) + 3]}, \text{ for smooth edges,}$$

561

$$f_0(\xi) = \xi \left[\kappa \frac{3\tilde{P}(48\rho + 5) - 64}{32\sqrt{1 - \xi^2}} - 2(\tilde{P} - 6\omega) \right] + \xi^3 \left[2\tilde{P} - \frac{\kappa(24\rho + 5)}{8\sqrt{1 - \xi^2}} \right] + \frac{\kappa\xi^5}{4\sqrt{1 - \xi^2}}, \text{ for sharp edges,}$$

$$f_0(\xi) = \frac{\xi}{8} [16(\xi^2 - 1)\tilde{P} + \kappa\sqrt{1 - \xi^2}(3 - 2\xi^2 + 24\rho) + 96\omega], \text{ for smooth edges,}$$

$$\begin{aligned}
 f_{2n}(\xi) &= \frac{\xi}{32(4n^2 - 1)} \left\{ \frac{\kappa \left\{ (32(4 - 5n^2)\rho\tilde{P} + n^2[64[\omega(1 - n^2) + 1] - 27\tilde{P}] + 15\tilde{P} - 32(\omega + 1)) \right\}}{(n^2 - 1)\sqrt{1 - \xi^2}\tilde{P}} \right. \\
 &\quad \left. + 96(\tilde{P} - 4\omega) \right\} + \frac{\xi^3}{8(1 - 4n^2)} \left(16\tilde{P} - \kappa \frac{24\rho + 7}{\sqrt{1 - \xi^2}} \right) + \frac{\kappa \xi^5}{(4 - 16n^2)\sqrt{1 - \xi^2}} \\
 &\quad + T_{2n-1}(\xi) \frac{\kappa(2n - 1)\{8[n(2n - 1) - 1]\rho + 3\} + 16[n(1 - 2n) + 1]\sqrt{1 - \xi^2}\tilde{P}}{32(1 - n)(1 - 4n^2)\sqrt{1 - \xi^2}} \\
 &\quad + T_{2n+1}(\xi) \frac{16[n(2n + 1) - 1]\sqrt{1 - \xi^2}\tilde{P} - \kappa(2n + 1)\{8[n(2n + 1) - 1]\rho + 3\}}{32(1 + n)(4n^2 - 1)\sqrt{1 - \xi^2}} \\
 &\quad + \frac{\kappa}{32\sqrt{1 - \xi^2}} \left[\frac{T_{2n+3}(\xi)}{n(2n + 3) + 1} + \frac{T_{2n-3}(\xi)}{n(2n - 3) + 1} \right] + 2n\omega U_{2n-1}(\xi), \text{ for sharp edges,} \\
 f_{2n}(\xi) &= \xi \frac{4(9 - 8\xi^2)\tilde{P} + \kappa\sqrt{1 - \xi^2}[2(\xi^2 - 12)\rho - 5] - 96\omega}{8(4n^2 - 1)} + \frac{\tilde{P}}{2} \left[\frac{T_{2n-1}(\xi)}{1 - 2n} \frac{T_{2n+1}(\xi)}{1 + 2n} \right] \\
 &\quad + U_{2n-1}(\xi) \frac{4n[8\omega n^2 - (\tilde{P} + 2\omega)] + \kappa\sqrt{1 - \xi^2}[1 + 2\rho(4n^2 - 1)]}{4(n^2 - 1)} \\
 &\quad + \frac{4\tilde{P}(n - 1) - \kappa\sqrt{1 - \xi^2}}{16} \left[\frac{U_{2n-3}(\xi)}{n(2n - 3) + 1} + \frac{U_{2n+1}(\xi)}{n(2n + 3) + 1} \right], \text{ for smooth edges.}
 \end{aligned}$$

562 In order to remove the spatial variable dependences from the series governing Eq. (37), it is multiplied by $T_m(\xi)/\sqrt{1 - \xi^2}$ or $T_m(\xi)$
 563 (with $m \in \mathbb{N}$) for sharp and smooth beam edges, respectively, and then integrated over the contact domain. By using results (44) and
 564 (45) leads to obtain the following eigensystem problem

$$\mathbf{A}(\tilde{P})\mathbf{c} = \mathbf{0}. \tag{38}$$

565 being

$$\mathbf{A}(\tilde{P}) = \begin{cases} [\mathbf{f}_m(\tilde{P}) \mid \mathbf{F}_{m,2n-1}(\tilde{P})], & \text{for even modes} \\ [\mathbf{g}_m(\tilde{P}) \mid \mathbf{G}_{m,2n}(\tilde{P})], & \text{for odd modes} \end{cases} \tag{39}$$

566 the system coefficients matrix and \mathbf{c} the Chebyshev coefficients vector. The symbol $|$ denotes concatenation. In particular, the coefficients
 567 $f_m, F_{m,2n-1}, g_m$ and $G_{m,2n}$ read

$$f_m = \mathbf{f}_1(\tilde{P}) \cdot \mathbf{t}_m \text{ Even}, \quad F_{m,2n-1} = \mathbf{f}_{2n-1}(\tilde{P}) \cdot \mathbf{t}_m \text{ Even}, \tag{40}$$

$$568 \quad g_m = \mathbf{g}_0(\tilde{P}) \cdot \mathbf{t}_m \text{ Odd}, \quad G_{m,2n} = \mathbf{g}_{2n}(\tilde{P}) \cdot \mathbf{t}_m \text{ Odd}, \tag{41}$$

569 being: For sharp edges:

$$\mathbf{t}_m \text{ Even} = \begin{bmatrix} t_{2,m} \\ t_{4,m} \\ t_{6,m} \\ t_{2n,m} \\ t_{2n-2,m} \\ t_{2n+2,m} \\ t_{2n-4,m} \\ l_{0,m} \\ l_{2,m} \\ l_{4,m} \\ l_{6,m} \\ l_{2n-2,m} \\ l_{2n,m} \\ r_{2(n-1),m} \end{bmatrix}, \quad \mathbf{f}_1(\tilde{P}) = \begin{bmatrix} \kappa \frac{\tilde{P}[3\rho(160\rho + 69) + 5] - 5(96\rho + 35)}{192(\tilde{P} + 5\omega)} \\ \kappa \frac{60\rho + 7 - \tilde{P}[3\rho(20\rho + 9) + 1]}{48(\tilde{P} + 5\omega)} \\ \frac{\kappa(\tilde{P} - 3\omega)}{192(\tilde{P} + 5\omega)} \\ 0 \\ 0 \\ 0 \\ 0 \\ \tilde{P} \left[\frac{19\tilde{P}}{15(5\rho - 1)\tilde{P} - 75} + 2\rho + \frac{49}{40} \right] - 2 \\ \tilde{P} \left[\frac{58\tilde{P}}{15(5\rho - 1)\tilde{P} - 75} + 6\rho + \frac{37}{10} \right] - 6 \\ \frac{5\tilde{P}(\tilde{P} - 3\omega)}{24(\tilde{P} + 5\omega)} \\ 0 \\ 0 \\ 0 \\ 0 \end{bmatrix}$$

$$f_{2n-1}(\tilde{P}) = \left[\begin{array}{l} \kappa \left\{ \frac{\tilde{P}^{n(n-1)} \{5\rho[4n(n-1)(16\rho+5) - 48\rho - 47] - 9\} + 60\rho - 12}{64n\{n[4n(n-2) + 1] + 3\}(\tilde{P} + 5\omega)} \right. \\ \left. \dots + \frac{5[4 + n(1-n)(16\rho+5)]}{64n(n-1)(\tilde{P} + 5\omega)} \right\} \\ \frac{\kappa(40\rho+3)(\tilde{P} + (2n-3)(2n+1)\omega)}{32(2n-3)(2n+1)(\tilde{P} + 5\omega)} \\ \frac{\kappa(\tilde{P} + (2n-3)(2n+1)\omega)}{64(2n-3)(2n+1)(\tilde{P} + 5\omega)} \\ \frac{\kappa}{32} \left[\frac{n(1-2n)+1}{3} - 8\rho \right] \\ \frac{\kappa}{32} \left[8\rho + \frac{n}{n(2n-3)} \right] \\ \frac{32n(2n+1)}{\kappa} \\ - \frac{32[n(2n-5)+3]}{32n(2n+1)} \\ \left\{ \tilde{P}^3 \frac{5n\{n[4n(n-2)(24\rho-1)\omega + 48\rho - 17] + 144\rho + 13\} - 6\omega}{8n[4n^2(n-2) + n + 3](\tilde{P} + 5\omega)} \right. \\ \left. \dots + \tilde{P}^2 \frac{n[120(n+3)\rho^2 + (65 - 85n)\rho - 3(n+1)] + 6}{8n[4(2-n)n^2 - n - 3](\tilde{P} + 5\omega)} \right. \\ \left. \dots + \frac{15n[4n^2(n-2)\omega + n + 3]}{n[4(2-n)n^2 - n - 3](\tilde{P} + 5\omega)} \right\} \\ \frac{5[(2n-3)(2n+1)\omega + \tilde{P}](\tilde{P} - 24\omega)}{4(2n-3)(2n+1)(5\omega + \tilde{P})} \\ \frac{5\tilde{P}^2(2n-3)(2n+1)\omega + \tilde{P}^3}{8(3-2n)(2n+1)(5\omega + \tilde{P})} \\ 0 \\ \frac{\tilde{P}}{4(1-n)} \\ \frac{\tilde{P}}{4n} \\ (2n-1)\omega \end{array} \right].$$

$$t_m \text{ Odd} = \begin{bmatrix} t_{-1,m} \\ t_{1,m} \\ t_{3,m} \\ t_{5,m} \\ t_{2n+1,m} \\ t_{2n-1,m} \\ t_{2n+3,m} \\ t_{2n-3,m} \\ l_{1,m} \\ l_{3,m} \\ l_{2n+1,m} \\ l_{2n-1,m} \\ z_{2n-1,m} \\ z_{1,m} \end{bmatrix}, \quad g_0(\tilde{P}) = \begin{bmatrix} \frac{\kappa}{64} \left(48\rho - \frac{64}{\tilde{P}} + 3 \right) \\ \frac{\kappa}{64} \left(96\rho - \frac{64}{\tilde{P}} + 7 \right) \\ -\frac{\kappa}{64} (48\rho + 5) \\ \frac{\kappa}{64} \\ 0 \\ 0 \\ 0 \\ 0 \\ 0 \\ \frac{\tilde{P}}{2} \\ \frac{\tilde{P}}{2} \\ 0 \\ 0 \\ 0 \\ 6\omega \end{bmatrix}.$$

$$\mathbf{g}_{2n}(\tilde{P}) = \begin{bmatrix} \frac{\kappa}{\tilde{P}} \frac{(128 - 64n^2 - 7\tilde{P})n^2 + 64(n^2 - 1)^2\rho\tilde{P} - 5\tilde{P} - 64}{64[n^2(4n^2 - 5) + 1]} \\ \frac{\kappa}{\tilde{P}} \frac{64(\rho\tilde{P} - 1)n^4 + [128 - (176\rho + 15)\tilde{P}]n^2 + (112\rho + 3)\tilde{P} - 64}{64[n^2(4n^2 - 5) + 1]} \\ \frac{3\kappa(16\rho + 3)}{64(4n^2 - 1)} \\ \frac{\kappa}{64(1 - 4n^2)} \\ \frac{1}{32}\kappa \left[\frac{1 - n(2n + 1)}{3} - 8\rho \right] \\ \frac{1}{32}\kappa \left[8\rho + \frac{n(2n + 1) - 1}{\kappa} \right] \\ \frac{32[n(2n + 3) + 1]}{\kappa} \\ \frac{32[n(3 - 2n) - 1]}{3\tilde{P}} \\ \frac{2(4n^2 - 1)}{\tilde{P}} \\ \frac{2(1 - 4n^2)}{\tilde{P}} \\ \frac{2(2n + 1)}{\tilde{P}} \\ \frac{2(1 - 2n)}{2n\omega} \\ \frac{6\omega}{1 - 4n^2} \end{bmatrix}$$

571 where t_{ij}, l_{ij}, r_{ij} and g_{ij} follows from Eqs. (42)–(45).
 572 For smooth edges:

$$\mathbf{t}_m \text{ Even} = \begin{bmatrix} r_{1,m} \\ r_{3,m} \\ r_{5,m} \\ r_{2n-1,m} \\ r_{2n+1,m} \\ r_{2n-3,m} \\ g_{0,m} \\ g_{2,m} \\ g_{4,m} \\ g_{2n-2,m} \\ g_{2n,m} \\ g_{2n-4,m} \end{bmatrix}, \quad \mathbf{f}_1(\tilde{P}) = \begin{bmatrix} \frac{\kappa}{48} \left(24\rho - \frac{16\tilde{P}}{5\omega + \tilde{P}} + 15 \right) \\ \frac{3[5\rho(16\rho + 7) + 1]\tilde{P} - 5(48\rho + 5)}{\kappa} \\ \frac{96(5\omega + \tilde{P})}{3\omega - \tilde{P}} \\ \kappa \frac{96(5\omega + \tilde{P})}{96(5\omega + \tilde{P})} \\ 0 \\ 0 \\ 0 \\ \frac{2\tilde{P}^2}{3(5\omega + \tilde{P})} - \frac{1}{8}(8\rho + 5)\tilde{P} + 1 \\ \frac{3}{80}\tilde{P} \left(80\rho - \frac{56\tilde{P}}{5\omega + \tilde{P}} + 51 \right) - 3 \\ \tilde{P} \frac{5(\tilde{P} - 3\omega)}{48(5\omega + \tilde{P})} \\ 0 \\ 0 \\ 0 \end{bmatrix}$$

$$f_{2n-1}(\tilde{P}) = \begin{bmatrix} \frac{\kappa}{8} \left[\frac{4(n-2)(n+1)\tilde{P}}{(3-2n)(2n+1)(5\omega+\tilde{P})} + \frac{1}{n(1-n)} + 1 \right] \\ 5\kappa \frac{(16\rho+1)[4n\omega(n-1)-3\omega+\tilde{P}]}{32(3-2n)(2n+1)(5\omega+\tilde{P})} \\ \frac{\kappa}{32} \frac{4(n+1)n\omega-3\omega+\tilde{P}}{(2n-3)(2n+1)(5\omega+\tilde{P})} \\ \frac{\kappa}{16} \left[8\rho + \frac{1}{(n-1)n} \right] \\ - \frac{1}{16n(2n+1)} \\ - \frac{4[4n(2n-5)+12]}{16n(2n+1)} \\ \tilde{P} \left[\frac{4(n-2)(n+1)\tilde{P}}{(2n-3)(2n+1)(5\omega+\tilde{P})} + \frac{1}{n-1} - \frac{1}{n} - 1 \right] \\ \frac{15[4(n-1)n\omega-3\omega+\tilde{P}](\tilde{P}-16\omega)}{16(2n-3)(2n+1)(5\omega+\tilde{P})} \\ \frac{5\tilde{P}[4(n-1)n\omega-3\omega+\tilde{P}]}{16(3-2n)(2n+1)(5\omega+\tilde{P})} \\ \frac{16(3-2n)(2n+1)(5\omega+\tilde{P})}{(1-2n)[\tilde{P}-8(n-1)n\omega]} \\ \frac{8(n-1)n}{\tilde{P}} \\ \frac{8n}{\tilde{P}} \\ \frac{8(n-1)}{\tilde{P}} \end{bmatrix},$$

$$t_m \text{ odd} = \begin{bmatrix} r_{2,m} \\ r_{4,m} \\ r_{2n-2,m} \\ r_{2n,m} \\ r_{2n+2,m} \\ g_{1,m} \\ g_{3,m} \\ g_{2n-1,m} \\ g_{2n-3,m} \\ g_{2n+1,m} \end{bmatrix}, \quad g_0(\tilde{P}) = \begin{bmatrix} \frac{\kappa}{8}(12\rho+1) \\ -\frac{\kappa}{32} \\ 0 \\ 0 \\ 0 \\ 0 \\ 6\omega - \frac{\tilde{P}}{2} \\ \tilde{P} \\ \frac{4}{\tilde{P}} \\ 0 \\ 0 \\ 0 \end{bmatrix}, \quad g_{2n}(\tilde{P}) = \begin{bmatrix} \frac{\kappa}{4} \frac{6\rho+1}{1-4n^2} \\ \frac{32(4n^2-1)}{\kappa} \\ -\frac{16[n(2n-3)+1]}{2(4n^2-1)\rho+1} \\ \kappa \frac{4(4n^2-1)}{\kappa} \\ -\frac{16[n(2n+3)+1]}{\tilde{P}-6\omega} \\ \frac{4n^2-1}{\tilde{P}} \\ \frac{4(1-4n^2)}{n(8\omega n^2-\tilde{P}-2\omega)} \\ \frac{4n^2-1}{\tilde{P}} \\ \frac{4(2n-1)}{\tilde{P}} \\ \frac{4(2n+1)}{\tilde{P}} \end{bmatrix},$$

where terms $g_{m,n}$ are defined according to Eq. (45).

Once matrix $A(\tilde{P})$ has been assembled using relations (40) and (41), its determinant provides the system characteristic equation, i.e. the buckling spectrum whose roots are the dimensionless buckling loads \tilde{P}_i .

A3. Integral terms for the problem solution

The integral terms involved in the problem solution are:

$$t_{n,m} = \int_{-1}^{+1} \frac{T_n(\xi)T_m(\xi)}{\sqrt{1-\xi^2}} d\xi = \begin{cases} \pi/2, & \text{if } n = m \neq 0, \\ \pi, & \text{if } n = m = 0, \\ 0, & \text{if } n \neq m \end{cases} \quad (42)$$

$$l_{n,m} = \int_{-1}^{+1} T_n(x)T_m(x) dx = \begin{cases} \frac{(1-m^2-n^2)[(-1)^{m+n}+1]}{n^4-2(m^2+1)n^2+(m^2-1)^2}, & \text{if } n+m \text{ even} \\ 0, & \text{otherwise.} \end{cases} \quad (43)$$

$$r_{n,m} = \int_{-1}^{+1} U_{n-1}(x)T_m(x) dx = \begin{cases} \frac{2n}{n^2-m^2}, & \text{if } n+m \text{ odd} \\ 0, & \text{if } n+m \text{ even} \end{cases} \quad (44)$$

$$g_{n,m} = \int_{-1}^{+1} \frac{U_n(x)T_m(x)}{\sqrt{1-x^2}} dx = \begin{cases} 0, & \text{if } n+m \text{ odd or } m > n \\ \pi, & \text{otherwise.} \end{cases} \quad (45)$$

581 **References**

- 582 Baraldi, D., Tullini, N., 2018. In-plane bending of Timoshenko beams in bilateral frictionless contact with an elastic half-space using a coupled FE-BIE method. *Eng. Anal. Bound. Elem.* 97, 114–130. 606
- 583 607
- 584 Bazant, Z.P., Cedolin, L., 2003. *Stability of Structures. Elastic, Inelastic, Fracture, and Damage Theories*. Dover Publications, Inc. 608
- 585 609
- 586 610
- 587 Biot, M.A., 1937. Bending of an infinite beam on an elastic foundation. *J. Appl. Mech.* 4, 1–7. 611
- 588 612
- 589 Biot, M.A., 1957. Folding instability of a layered viscoelastic medium under compression. *Proc. R. Soc. Lond. A* 242 (1231), 444–454. 613
- 590 614
- 591 Falope, F.O., Lanzoni, L., Radi, E., Tarantino, A.M., 2016. Thin film bonded to elastic orthotropic substrate under thermal loading. *J. Strain Anal. Eng.Des.* 51 (4), 256–269. 615
- 592 616
- 593 617
- 594 Falope, F.O., Lanzoni, L., Tarantino, A.M., 2018. Modified hinged beam test on steel fabric reinforced cementitious matrix (SFRCM). *Composites Part B* 146, 232–243. 618
- 595 619
- 596 Foraboschi, P., 2009. Buckling of a laminated glass column under test. *Struct. Eng.* 87 (1), 2–8. 620
- 597 621
- 598 Gallagher, A.P., 1974. Buckling of a beam under axial compression with elastic support. *Stud. Numer. Anal.* 137–150. 622
- 599 623
- 600 Hetényi, M., 1971. *Beams on Elastic Foundation: Theory with Applications in the Fields of Civil and Mechanical Engineering*. University of Michigan. 624
- 601 625
- 602 Kachanov, M.L., Shafiro, B., Tsukrov, I., 2013. *Handbook of Elasticity Solutions*. Springer Science & Business Media. 626
- 603 627
- 604 Lanzoni, L., Radi, E., 2016. A loaded Timoshenko beam bonded to an elastic half plane. *Int. J. Solids Struct.* 92, 76–90. 628
- 605 629
- Mace, B.R., Manconi, E., 2012. Wave motion and dispersion phenomena: veering, locking and strong coupling effects. *J. Acoust. Soc. Am.* 131 (2), 1015–1028.
- Mason, J.C., Handscomb, D.C., 2002. *Chebyshev Polynomials*. Chapman and Hall/CRC.
- Muskhelishvili, N.I., 2013. *Some Basic Problems of the Mathematical Theory of Elasticity*. Springer Science & Business Media.
- Reynolds, O., 1886. IV. On the theory of lubrication and its application to Mr. Beauchamp tower's experiments, including an experimental determination of the viscosity of olive oil. *Philos. Trans. R. Soc.London* 177, 157–234.
- Ruta, G.C., Elishakoff, I., 2006. Buckling of a column on a Wiegardt foundation. *ZAMM* 86 (8), 617–627.
- Shield, T.W., Kim, K.S., 1992. Beam theory models for thin film segments cohesively bonded to an elastic half space. *Int. J. Solids Struct.* 29, 1085–1103.
- Smith, T.E., 1969. Buckling of a beam on a Wiegardt-type elastic foundation. *ZAMM* 49 (11), 641–645.
- Tezzon, E., Tullini, N., Lanzoni, L., 2016. A coupled FE-BIE model for the static analysis of Timoshenko beams bonded to an orthotropic elastic half-plane. *Eng. Anal. Bound. Elem.* 71, 112â;128.
- Timoshenko, S.P., Gere, J.M., 1961. *Theory of Elastic Stability*. McGraw-Hill, New York.
- Tullini, N., Tralli, A., Baraldi, D., 2012. Buckling of Timoshenko beams in frictionless contact with an elastic half-plane. *J. Eng. Mech.* 139 (7), 824–831.
- Tullini, N., Tralli, A., Baraldi, D., 2013. Stability of slender beams and frames resting on 2D elastic half-space. *Arch. Appl. Mech.* 83 (3), 467–482.
- Wiegardt, K., 1922. Über den balken auf nachgiebiger unterlage. *ZAMM* 2 (3), 165–184.